A COMPREHENSIVE STUDY ON THEORETICAL AND EXPERIMENTAL EFFECTS OF NICOTINIC ACID AND PICOLINIC ACID ON THE STRUCTURE AND STABILITY OF HUMAN SERUM ALBUMIN[**]

K. G. Chegini [1], S. M. Sadati [2], A. Rahbarimehr [2], P. Yaghmaei [2], A. Farasat [3], N. Gheibi [1*]

[1] Cellular and Molecular Research Center, Qazvin University of Medical Sciences, Qazvin, Iran; e-mail: ngheibi@qums.ac.ir
[2] Islamic Azad University of Science and Research Branch, Faculty of Basic Sciences, Tehran, Iran
[3] Qazvin University of Medical Sciences, Department of Biotechnology, Qazvin, Iran

The interaction of nicotinic acid (Nic) and picolinic acid (Pic), as two pyridine carboxylic acids, with human serum albumin (HSA) as a major transport protein in the blood was investigated using UV-Vis, fluorimetry, circular dichroism (CD), and molecular docking studies. The melting point (T_m) and $\Delta G^0_{(298K)}$ of HSA, as two thermodynamic parameters, were obtained from thermal denaturation of HSA with and without the presence of Nic and Pic. T_m values of 332.5, 336.4, and 333.9 K, and ΔG^0_{298K} of 97.4, 99.9, and 118.9 kJ/mol were recorded for HSA alone and following incubation with Nic and Pic, respectively. In chemical denaturation experiments utilizing guanidine hydrochloride (GuHcl), value of ΔG^0_{H2O} of 12.5, 16, and 15.3 kJ/mol, $[Ligand]_{1/2}$ of 2.2, 2.4, and 2.3 M, and m of 5.6, 6.6, and 6.6 kJ/(mol · M) were recorded, respectively. The results of CD, UV-Vis spectroscopy, and molecular dynamics (MD) simulations showed that the binding of Nic and Pic to HSA induced conformational changes in HSA. Furthermore, the study of molecular docking indicated that the binding affinity of the Nic and Pic to site I (subdomain IIA) is greater than that of site II (subdomain IIIA) of HSA. These results provide valuable insights into the binding mechanisms of Nic and Pic to a plasma protein that is known to play an important role in the delivery of drugs to target organs.

Keywords: *human serum albumin, stability, molecular docking, molecular dynamics.*

ТЕОРЕТИЧЕСКОЕ И ЭКСПЕРИМЕНТАЛЬНОЕ ИССЛЕДОВАНИЕ ВЛИЯНИЯ НИКОТИНОВОЙ И ПИКОЛИНОВОЙ КИСЛОТ НА СТРУКТУРУ И УСТОЙЧИВОСТЬ СЫВОРОТОЧНОГО АЛЬБУМИНА ЧЕЛОВЕКА

K. G. Chegini [1], S. M. Sadati [2], A. Rahbarimehr [2], P. Yaghmaei [2], A. Farasat [3], N. Gheibi [1*]

УДК 543.42:547.962.3

[1] Центр клеточных и молекулярных исследований, Университет медицинских наук, Казвин, Иран; e-mail: ngheibi@qums.ac.ir
[2] Исламский университет Азада, Тегеран, Иран
[3] Университет медицинских наук, Казвин, Иран

(Поступила 19 февраля 2018)

Взаимодействие никотиновой и пиколиновой кислот с сывороточным альбумином человека (САЧ) — основным транспортным белком крови — исследовано с использованием методов УФ и видимой спектроскопии, флуориметрии, кругового дихроизма и молекулярного докинга. Два термодинамических параметра САЧ – точка плавления (T_m) и $\Delta G^0_{(298K)}$ – получены из данных по термическому разложению САЧ в присутствии и в отсутствие никотиновой и пиколиновой кислот. Для

[**]Full text is published in JAS V. 86, No. 4 (http://springer.com/10812) and in electronic version of ZhPS V. 86, No. 4 (http://www.elibrary.ru/title_about.asp?id=7318; sales@elibrary.ru).

САЧ без кислот и после инкубации САЧ с никотиновой или пиколиновой кислотой получены T_m = = 332.5, 336.4 и 333.9 К и ΔG^0_{298K} = 97.4, 99.9 и 118.9 кДж/моль соответственно. В экспериментах по химической денатурации с использованием гидрохлорида гуанидина ΔG^0_{H2O} = 12.5, 16 и 15.3 кДж/моль, $[лиганд]_{1/2}$ = 2.2, 2.4 и 2.3 М, m = 5.6, 6.6 и 6.6 кДж/(моль·М). Результаты, полученные методами кругового дихроизма, УФ-видимой спектроскопии и молекулярной динамики, показывают, что связывание никотиновой и пиколиновой кислот с САЧ вызывает конформационные изменения в САЧ. Исследование методами молекулярного докинга показывает, что сродство связывания никотиновой и пиколиновой кислот с сайтом I (поддомен IIA) больше, чем с сайтом II (поддомен IIIA) САЧ.

Ключевые слова: *сывороточный альбумин человека, стабильность, молекулярный докинг, молекулярная динамика.*

Introduction. Pyridine carboxylic acid and its derivatives constitute several natural and synthetic products with special interest for medicinal chemists due to their physiological properties [1]. Currently, they have applications in biodegradable polymers and pharmaceuticals and as raw material for food additives. Nicotinic acid (3-pyridine carboxylic acid) and picolinic acid (2-pyridine carboxylic acid) are important chemicals used in the food and drug industries [1].

Nicotinic acid (also known as niacin, or vitamin B3) is a water-soluble vitamin with good biological activities and versatile bonding modes (Fig. 1a). It plays a nutritional role as a vitamin, a deficiency of which results in pellagra. This vitamin is involved in a wide range of biological processes, including production of energy, synthesis of fatty acids and steroids, signal transduction, regulation of gene expression, and maintenance of genomic integrity. It serves as a precursor to various forms of coenzyme nicotinamide adenine dinucleotide and a broad spectrum of lipid-based drugs applied to lower the cholesterol level [2].

Nicotinic acid derivatives are routinely used as antimicrobial, fungicidal, agricultural and industrial chemicals and have mostly been documented for their wide variety of pharmacological activities such as antimicrobial, analgesic, anti-inflammatory, anti-HIV, and antitubercular [3–7]. Picolinic acid is a white crystalline solid (Fig. 1a) with several applications in the pharmaceutical and chemical industries. It works as a chelating agent of molybdenum, zinc, chromium, manganese, and iron copper elements in the human body. Picolinic acid is a precursor for the production of pharmaceuticals such as local anesthetics and nutritional supplements such as metal salts [1]. Various biological media including, human milk, blood serum, cerebrospinal fluid (CSF), cell culture supernatants, intestinal homogenates, and pancreatic juice contain high levels of picolinic acid [8]. It is also used for quantitative detection of calcium. Picolinic acid is biosynthezed from tryptophan in the kidneys and liver, then stored and secreted in the pancreas and the intestine, respectively [9].

As the functional modules of the cell and the most abundant macromolecules in living systems, investigation of proteins is of extreme importance in life sciences, biochemistry and clinical medicine. Human serum albumin (HSA) is the most abundant protein in plasma, characterized by extraordinary ligand binding capacity and providing a depot and carrier for many compounds (Fig. 1b) [10, 11].

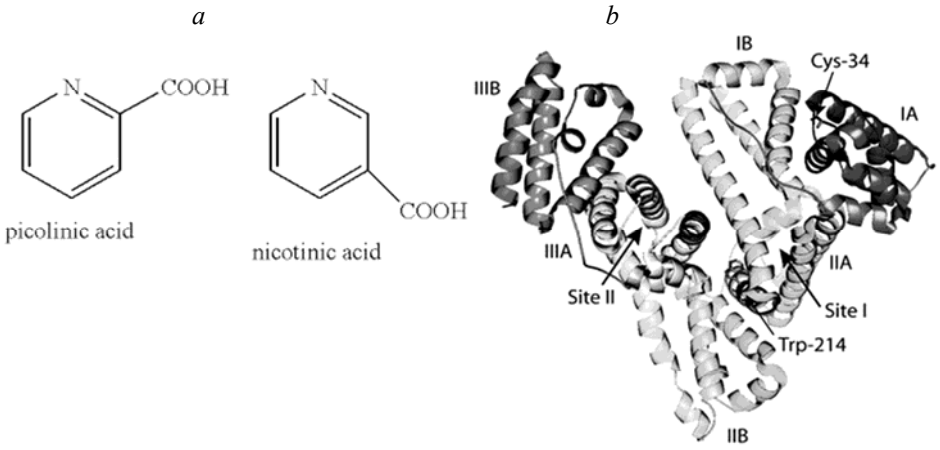

Fig. 1. Nicotinic acid, picolinic acid (a), and human serum albumin structures (b).

The globular protein of HSA is a single chain with 585 amino acid residues, comprised of three similar domains (I, II, and III), each of which has two subdomains (IA, IB, etc.). A variety of ligands has been found to bind the two hydrophobic pockets in subdomains IIIA and IIA (site II and site I, respectively) [12–14].

The interaction of metabolites with serum albumin can elucidate the properties of metabolite–protein complexes and provide useful information about the structural features that determine the therapeutic effectiveness of metabolites. Therefore, studies on this aspect of HSA have been an interesting research field in the life sciences.

To the extent our knowledge, the interaction of Nic and Pic to HSA has not been previously reported. Herein we demonstrated the binding of Nic and Pic to HSA and also the thermodynamic of their interactions. In order to attain these objectives, we plan to carry out a detailed investigation of Nic, Pic–HSA association using UV-Vis absorption, circular dichroism (CD) in combination with theoretical molecular docking and molecular dynamics simulations analysis. We believe that the results of this study may provide valuable data with regards to Nic- and Pic-related drug delivery and drug design.

Material and methods. Human serum albumin (fatty acid-free, 20%), nicotinic acid, picolinic acid, and guanidine hydrochloride (GuHcl) were purchased from Sigma-Aldrich (St. Louis, MO, USA) and used without further purification. All the compounds and proteins were dissolved in 50 mM phosphate buffer solution (pH 6.8) individually and kept in the dark at 0–4°C. All other chemicals were of analytical grade. Double-distilled water was used throughout. pH measurements were carried out with a digital pH-meter with a combined glass-calomel electrode.

Chemical denaturation of HSA by GuHCl. Guanidine hydrochloride is generally used for chemical denaturation of HAS; 0.4 ml of protein solution containing 40 μM HSA was incubated with 100 μM of Nic or Pic. These solutions were titrated separately by successive addition of 10 ml GuHcl 8 M. Conformational change of the protein was evaluated by measuring the optical density (OD) at the wavelength 280 nm using a UV-Vis spectrophotometer (BioRad, USA) at room temperature.

UV-Vis spectra of HSA following Nic and Pic treatment. UV-Vis absorption spectra were measured on an Agilent UV-Vis spectrophotometer Model 8453, using a 1.0 cm quartz cell. Briefly, 40 μM HSA in 50 mM PBS buffer solution was assessed at the wavelength range of 200–300 nm with gradual addition of Nic, Pic, and buffer in native protein titrations. Samples were left to settle for 5 min. After each injection, the Nic concentration range was 0, 2, 4, 6, 8, and 10 μM, and the Pic concentrations were 0, 1, 2, 3, 4, and 5 μM.

Circular dichroism (CD) measurements were recorded with a spectropolarimeter (Aviv, Model 215, USA) using a 0.1 cm quartz cell. HSA at a concentration of 40 μM was pipetted into a 0.3 ml cell and incubated with the appropriate amount of Nic and Pic solutions for 5 min. CD spectra of the sole HSA and its incubation with different concentrations of Nic (0, 3, 6, and 10 μM) and Pic (0, 3, 6, and 10 μM) at far-UV region (190–260 nm) and near-UV region (260–320 nm) were measured in a quartz cuvette with a path length of 1.0 nm in nitrogen atmosphere.

Molecular docking. The geometries of Nic and Pic were obtained from PubChem, and the crystal structure of human serum albumin (entry code: 4K2C) was downloaded from the PDB bank (http://www.rcsb.org). Picolinic acid and nicotinic acid molecular dockings to HSA were accomplished using AutoDock Vina [15] by a pliable docking method with the flexibility of some receptor side chains and the ligand. The graphical interface AutoDock Tools 1.5.6 [16] was applied preliminarily to add polar hydrogen atoms to the protein in order to characterize the ligand permissible torsions and ascertain the search area coordinates. At that point the IIA and IIIA domains docking is done utilizing a grid framework size of 26×42×34 along the *X*, *Y*, and *Z* axes with 1 Å spacing. AutoDock Vina provided the lowest (most negative) binding energy of Pic 2-Pro, Pic3-Pro, Nic 2-Pro, and Nic 3-Pro complexes for the docking conformation, which was considered as the primary conformation for MD simulation.

Molecular dynamics of picolinic acid/nicotinic acid and HSA. The MD method estimated the conformational changes of picolinic acid/nicotinic acid and HSA complexes via GROMOS96 43a1 force field and the GROMACS 4.5.4 package software [17]. The complexes generated by molecular docking were located approximately in a periodic box full of water molecules. The topology parameters of HSA were provided using the Gromacs program. The Picolinic and nicotinic acid topology parameters were created by means of the Dundee PRODRG server [18]. The complex was immersed in a box filled with simple point charge water molecules. In order to minimize the energy, the steepest descent method of 10000 steps followed by the conjugate gradient method for 10,000 steps was utilized to release the conflicting contacts. The system equilibration phase (position-restrained dynamics simulation, NPT, and NVT) was performed at 300 K for 200 ps,

which was followed by an MD production run for 20 ns [19, 20]. During the MD simulation, the atomic coordinates were recorded every 2.0 ps for analysis.

Results and discussion. *Chemical and thermal denaturation.* Denaturation of HSA was induced by incubating in the absence or presence of Nic and Pic with various concentrations of GuHcl until equilibrium was achieved. The extent of unfolding transition of HSA is monitored by changes in UV-Vis absorption at 280 nm. The obtained data were normalized and analyzed according to the standard Pace equation [21, 22]:

$$K = f_{obs} - f_n/f_u - f_n, \quad (1)$$

where f_{obs} are the observed value of the signal at a given denaturant concentration, and f_n and f_u are the values of native and unfolded protein, respectively. From these measurements, values of $\Delta G_{N\text{-}D}$ for a two-state process were determined using the equation

$$\Delta G_{N\text{-}D} = -RT\ln K. \quad (2)$$

As illustrated by the sigmoidal curves in the plot, GuHcl unfolding transition of HSA in the absence and presence of Nic and Pic is cooperative and coincidental. Thus, GuHcl-induced unfolding of HSA can be explained by a simple two-state model:

$$\Delta G_{N\text{-}D} = \Delta G_{H2O} - m[D], \quad (3)$$

where ΔG_{H2O} is the free energy of the protein folding in water (in the absence of denaturant) as the criterion of conformation stability, and $\Delta G_{N\text{-}D}$ is the free energy at different concentrations of denaturant, where m is the slope of the ΔG_{N-D} vs [D] plot, and D is the denaturant concentration [23].

The use of the linear extrapolation method in secondary plots, where ΔG_{N-D} is linearly relevant to the denaturant concentration, is a simple method for calculating the protein stability and thermodynamic parameters such as $[Ligand]_{1/2}$, ΔG^0_{H2O}, and m for HSA alone and its treatment by Nic and Pic obtained: $[Ligand]_{1/2}$ = 2.2, 2.4, and 2.3 M; ΔG^0_{H2O} = 12.5, 16, and 15.3 kJ/mol; m = 5.68, 6.68, and 6.66 kJ/(mol · M), respectively [24] (Fig. 2a).

Thermal stability is the stability of a molecule at high temperatures. A molecule with greater stability has more resistance to denaturation at high temperatures [25]. Figure 2b elucidates the analysis method for a thermal unfolding curve of HSA in the absence and presence of Nic and Pic; from these sigmoid, the HSA melting temperature (T_m), the temperature at which the magnitude of ΔG equals zero, can be determined. T_m and ΔG^0_{298K}, as two thermodynamic parameters, were obtained for HSA, with and without the presence of Nic and Pic. T_m = 332.5, 336.4, and 333.9 K, and ΔG^0_{298K} = 97.4, 99.9, and 118.9 kJ/mol were reported for the HSA alone and incubated with Nic and Pic, respectively.

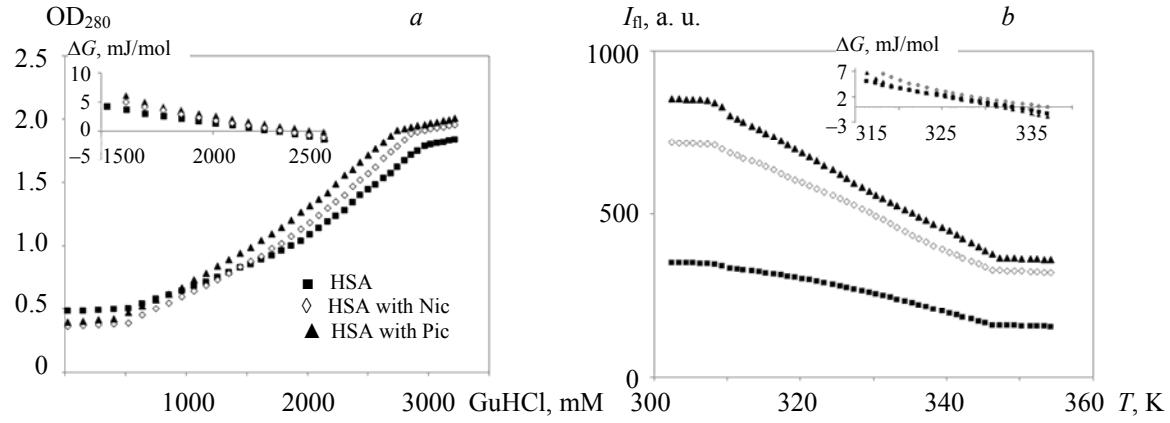

Fig. 2. Chemical denaturation of HSA, HSA with Nic and HSA with Pic by UV-Vis absorbance (OD_{280}). Inset: free energy change (ΔG) versus GuHcl concentration for the unfolding transition of HSA in the presence of Nic and Pic and in the absence of these compounds (a). Thermal denaturation of HSA, HSA with Nic and HSA with Pic by fluorescence spectroscopy (λ_{ex} = 280 nm). Inset: free energy change (ΔG) versus temperature (K) for the unfolding transition of HSA in the presence of Nic and Pic and in the absence of these compounds (b).

UV-Vis absorption measurement. To explore the effect of Nic and Pic on the conformation changes in HSA, UV-Vis absorption spectra measurement was performed. The structural changes of protein with ligands can be processed by this method [26]. The spectra recorded for HSA indicate a gradual decrease in absorption intensity with gradual increment of Nic and Pic concentrations.

Circular dichroism analysis. The conformational aspects of proteins and their binding may be studied using CD with different dyes. Depending on the nature of the probe, the secondary and/or tertiary structure of the proteins may be perturbed due to the interaction with small molecules [27, 28]. The effects of Nic and Pic on the structure of HSA were investigated by CD spectra in far- and near-UV regions. The far-UV CD spectra of HSA exhibited two negative minima at around 208 and 222 nm, characterizing the α-helical structure of HSA [27]. The interaction between Nic, Pic, and HSA caused an increase in the band intensities without any significant shift in the peaks (Fig. 3). Aromatic amino acids allow the near-UV CD spectra of HSA in the range 260–320 nm to be recorded. Increasing concentrations of Nic and Pic, led to a decrease in the peak at 280 nm (Fig. 3).

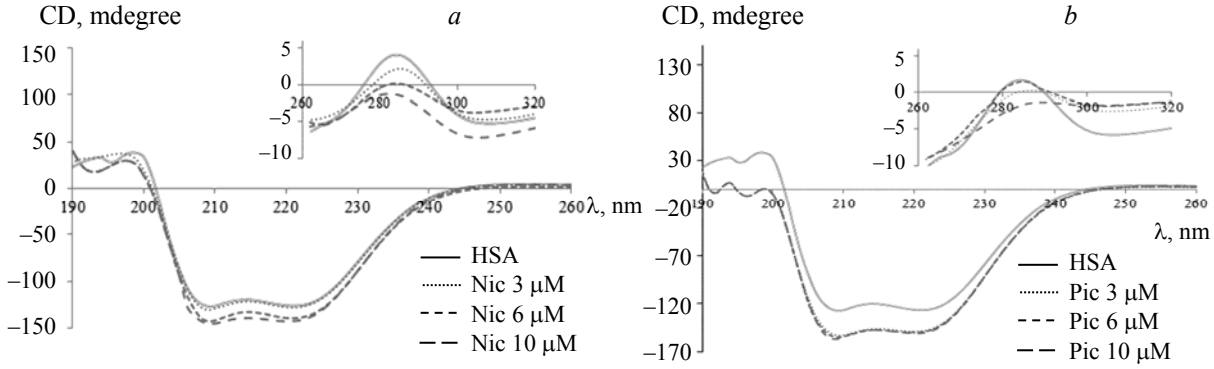

Fig. 3. Far UV-CD spectra of HSA in the absence and presence of nicotinic acid (T = 298 K, pH 6.8). [HSA] = 40μM. The concentration of nicotinic acid was 0, 3, 6, and 10 μM. Inset: Near-UV CD spectra of HSA in the absence and presence of nicotinic acid (T = 298 K, pH 6.8) (a). Far-UV CD spectra of HSA in the absence and presence of picolinic acid (T = 298 K, pH 6.8). [HSA] = 40 μM. The concentration of picolinic acid was 0, 3, 6, and 10 μM. Inset: Near-UV CD spectra of HSA in the absence and presence of nicotinic acid (T = 298 K, pH 6.8) (b).

Molecular docking and molecular dynamics. Molecular docking was performed to evaluate the interaction of Nic and Pic with specific binding sites on HSA. The binding locations of Nic and Pic on the HSA molecule are of great importance since information on the binding of proteins and ligands can help us understand their function and efficacy as potential therapeutic agents [29].

An important option which is accessible on AUTODOCK VINA docking software is selective side-chain residue flexibility [30]. The purpose of this approach is to provide a more realistic ligand-protein interaction environment, with no remarkable increase in computer processing time, and the receptor conformational changes, which may have substantial implications with regards to the selectivity of the ligand, indicate that the incorporating receptor flexibility plays a great role in computational drug design [31]; this is the method that was used in this study. To evaluate the structural modifications induced by the ligand binding (Nic and Pic), molecular dynamics simulations were done for free HSA (subdomain II and III) and the four complexes Pic 2-HSA, Pic 3-HSA, Nic 2-HSA, and Nic 3-HAS, and the results were eventually compared.

The root mean, square fluctuations (RMSF), root mean square deviations (RMSD), and the secondary structure were evaluated. Based on structural properties, the HSA protein stability could be evaluated during the time of simulation. The RMSD evolution time from the primary structure for five runs of simulations were measured. RMSDs of the protein C_α atoms are illustrated in Fig. 4, which is the representation of RMSD for four complexes. The free protein and the protein involved in the complex attained suitable stability after 2 ns, indicating system equilibration. The RMSD values of the C_α-atoms of HSA and the aforementioned complexes showed equilibration and oscillation close to an average value for all the systems and stability up to the end of the simulation process.

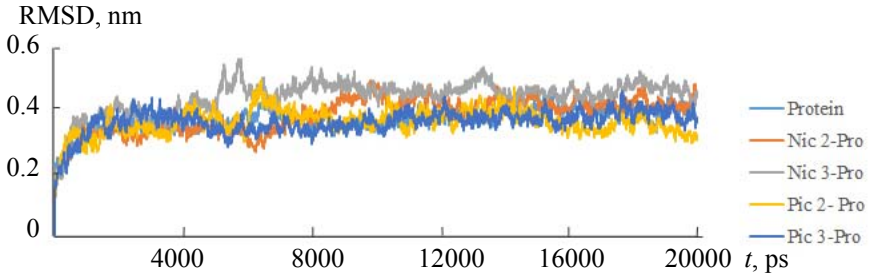

Fig. 4. RMSD values of carbon-α of free HSA and HSA in complex with nicotinic acid and Picolinic acid. Free HSA (light blue), Nic 2-Pro (orange), Nic 3-Pro (grey), Pic 2-Pro (yellow), and Pic 3-Pro (dark blue).

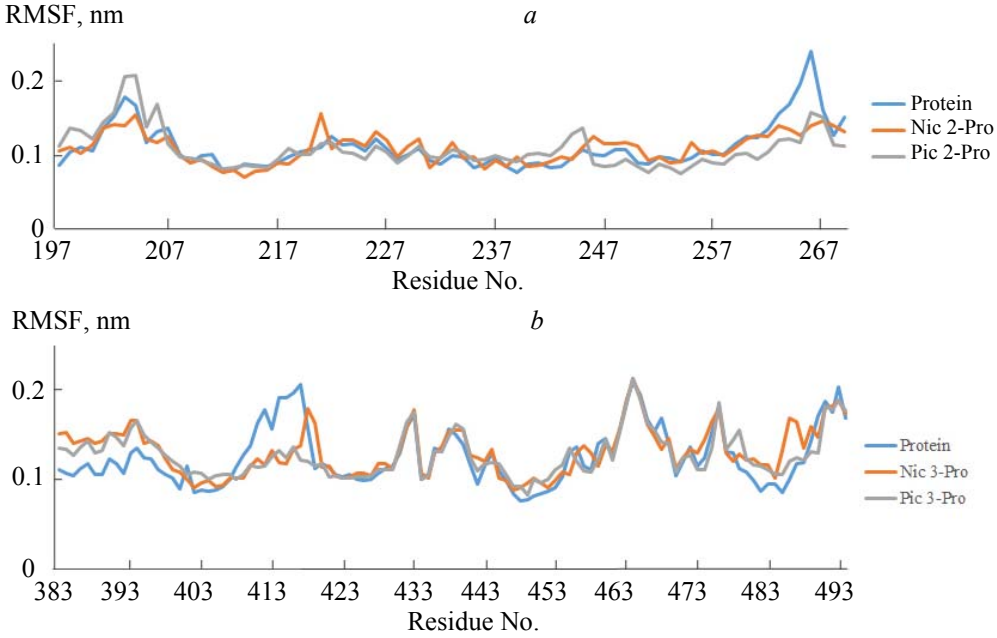

Fig. 5. Root mean square fluctuation (RMSF) of free HSA and HSA in complex with nicotinic acid and picolinic acid. In subdomain IIA, Free HSA (blue), Nic-Pro (orange), and Pic-Pro (grey) (a); In subdomain IIIA, Free HSA (blue), Nic-Pro (orange), and Pic-Pro (grey) (b).

RMSF is applied to achieve flexibility information. To recognize the molecule flexible regions, RMSFs of the protein C_α atoms are shown in Fig. 5. As the figure indicates, the RMSF for the free protein and the protein involved in the complex with ligands have a similar tendency in which the residues 261–268 and 406–419 have the highest values of the RMSF in subdomains IIA and IIIA, respectively. Due to molecular movement limitations caused by ligand binding, the free protein shows higher RMSF values toward the protein with ligands involved in the complex.

The secondary structure analysis was performed using the DSSP program [32]. The secondary structure of the free protein and that in the complex with ligands are illustrated in Fig. 6. During the 20 ns MD simulation, the secondary structure of the bound HSA and the free protein were preserved despite the small changes at some points.

As presented in Fig. 7a, after molecular dynamics, in site I the Pic-HSA complex is formed by hydrophobic interaction between them. As for the Nic-HSA complex, the interface was established by hydrogen bonding of His242 and hydrophobic interaction (Fig. 7c). In site II, the Pic-HSA complex is formed by hydrogen bonding of Tyr401 and hydrophobic interaction (Fig. 7b). As for the Nic-HSA complex, the interface was established by hydrophobic interaction (Fig. 7d). After docking and molecular dynamics, the best possible condition was achieved in Pic 2 and Nic 2 with HSA. The affinity of the Pic 2 and Nic 2 with HSA was –4.8 and –4.6 kcal/mol, respectively. These results indicated that Nic and Pic bind strongly to the large hydrophobic cavity present on HSA at subdomain IIA of site I. In the past decade, HSA has been vastly used in

biotechnology as a carrier for drug delivery. At least six regions have been explored in HSA for non-covalent binding of ions and small molecules [33, 34].

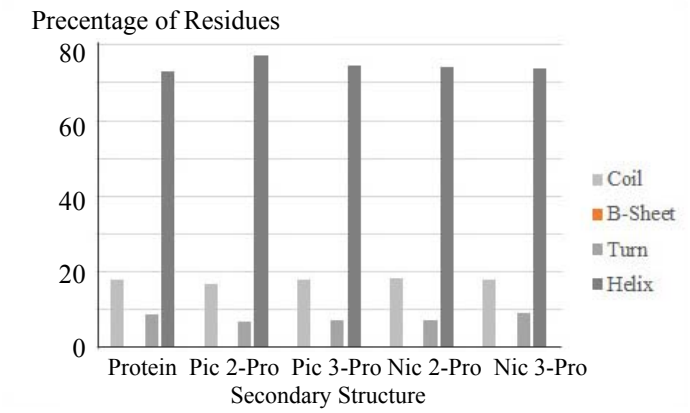

Fig. 6. Secondary structures a s a function of time for 20 ns simulation, at 300 K for free HSA and HSA in complex with nicotinic acid and picolinic acid. Different colors were applied to distinguish the secondary structure types.

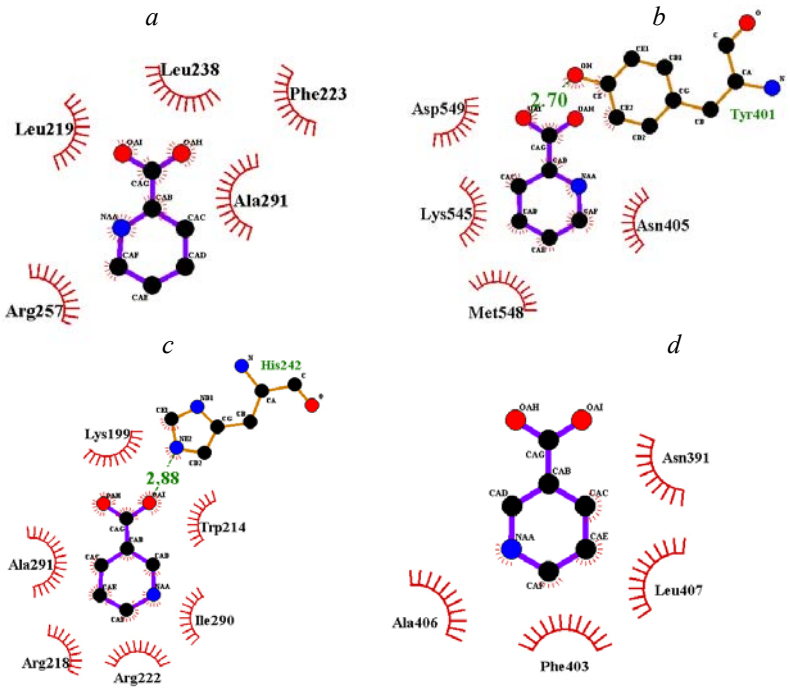

Fig. 7. Best docked conformations of Pic 2-Pro complex (a); Pic 3-Pro complex (b); Nic 2-Pro complex (c); Nic 3-Pro complex (d).

In this study, the interaction of Nic and Pic with HSA was investigated by using spectroscopic methods, molecular docking, and molecular dynamics. The stability of proteins in the solution is a main area of interest for biologists and pharmacologists [35]. In determining the stability and folding pathway of proteins, the denatured and native states of proteins are equally important [36]. Traditionally, guanidine hydrochloride is the most common denaturant for the study of protein stability and folding pathways [37]. On the other hand, hydrogen bonds in proteins are formed by using urea as denaturant [38]. To achieve this goal, we have measured some thermodynamic parameters associated with the unfolding process of HSA using thermal spectroscopy and chemical denaturation by GuHCl. The thermodynamic data acquired via chemical and thermal unfolding processes indicated that Nic and Pic induced conformational stability in HSA (Table 1). Also, another study showed that AuNPs increase the melting temperature of HSA [39].

TABLE 1. Calculated Thermodynamic Parameters from Chemical and Thermal Denaturation Curves of Sole HSA and its Interaction with Nicotinic Acid and Picolinic Acid

Sample	Chemical denaturation			Thermal denaturation	
	$[Ligand]_{1/2}$, M	ΔG_{H2O}, kJ/mol	m, kJ/mol	T_m, K	ΔG_{298K}, kJ/mol
HSA	2.2	12.5	5.6	332.5	97.4
HSA with Nic	2.4	16	6.6	336.4	99.9
HSA with Pic	2.3	15.3	6.6	333.9	118.9

UV-Vis absorption measurement is a very simple method employed to evaluate the structural changes and complex formation in proteins [40, 41]. In this study the interaction between Nic, Pic and HAS, formation of a ground state complex, and change in the microenvironment were indicated. To ascertain the possible influence of Nic and Pic binding on the secondary structure of HSA, far-UV CD measurement was performed at different concentrations of these compounds. The interaction between Nic, Pic, and the HSA caused an increase in the band intensities without any significant shift of the peaks, indicating that the dye induces an increase in the helical structure content of HSA. The increase in the band intensities is an indication of stabilization of the HSA upon binding with these compounds (Fig. 3) [42]. However, the CD spectra of HSA in the presence or absence of Nic and Pic are similar in shape, signifying that the structure of HSA is also predominantly α-helical.

In a study by Zhang et al. [43], it was shown that interaction of miriplatin with HSA induces relatively obvious changes in the secondary structure of HSA. Their far-UV CD results showed that the binding interaction of miriplatin with HSA induced the mentioned changes. As shown in Fig. 3, the interaction between Nic, Pic, and HSA caused only a decrease in band intensity of the near-UV CD (260–320 nm), which implles that binding of Nic and Pic to HSA induces stability of the tertiary structure.

Many studies have confirmed the IIA and IIIA subdomains as target sites for docking process. This is because the aforementioned sites are considered as initial drug binding sites. Any experiment that examines the ligand binding site besides drug-binding sites I and II could be beneficial for choosing the best position for docking simulation. To evaluate the structural changes caused by the ligands (picolinic and nicotinic acid) binding, the MD simulations for free HSA and Nic/Pic subdomains IIA and IIIA binding were carried out, and the results were compared. The results indicated that Nic and Pic bind strongly to the large hydrophobic cavity present on HSA at subdomain IIA of site I. The binding site of HSA was studied to explore the nature of the residues that comprise the site.

Conclusion. The docking and molecular dynamic in line with thermodynamic and structural results revealed that Nic and Pic could stabilize the protein through strong interaction with the large hydrophobic cavity present on HSA at subdomain IIA of site I. The verification of these two compound binding sites and the hydrophobic nature of their interaction with HSA, as the most important carrier protein in the serum, could offer new insights and valuable information into the mechanism of the biological effects and function of Nic and Pic in biological processes in the human body.

Acknowledgment. The financial support of this work by Qazvin University of Medical Science is gratefully acknowledged.

Declaration of interest. The authors report no conflicts of interest. The authors alone are responsible for the content and writing of the paper.

REFERENCES

1 M. D. Waghmare, K. L. Wasewar, S. S. Sonawane, D. Z. Shende, *Sep. Purif. Technol.*, **120**, 296–303 (2013).
2. L. A. Carlson, *J. Int. Med.*, **258**, 2, 94–114 (2005).
3. N. Khunnawutmanotham, N. Chimnoi, P. Saparpakorn, P. Pungpo, S. Louisirirotchanakul, S. Hannongbua, S. Techasakul, *Molecules*, **12**, 2, 218–230 (2007).
4. M. C. Lourenço, M. V. de Souza, A. C. Pinheiro, M. d. L. Ferreira, R. S. Gonçalves, T. C. M. Nogueira, M. A. Peralta, *Arkivoc*, **15**, 181–191 (2007).
5. W. L. Mitchell, G. M. Giblin, A. Naylor, A. J. Eatherton, B. P. Slingsby, A. D. Rawlings, K. S. Jandu, C. P. Haslam, A. J. Brown, P. Goldsmith, *Bioorg. Med. Chem. Lett.*, **19**, No. 1, 259–263 (2009).
6. N. B. Patel, F. M. Shaikh, *Saudi Pharm. J.*, **18**, 3, 129–136 (2010).

7. M. Pavlova, A. Mikhalev, M. Kon'shin, M. Y. Vasil'eva, L. Mardanova, T. Odegova, M. Vakhrin, *Pharm. Chem. J*., **35**, 12, 664–666 (2001).
8. R. Grant, S. Coggan, G. Smythe, *Int. J. Tryptophan Res*., **2**, 71 (2009).
9. J. A. Fernandez-Pol, P. D. Hamilton, D. J. Klos, *Anticancer Res.*, **21**, 2A, 931–957 (2001).
10. P. Lee, X. Wu, *Curr. Pharm. Des*., **21**, 14, 1862–1865 (2015).
11. C. Müller, R. T. Farkas, F. Borgna, R. M. Schmid, M. Benešová, R. Schibli, *Bioconjug. Chem*., **28**, 9, 2372–2383 (2017).
12. O. Dömötör, T. Tuccinardi, D. Karcz, M. Walsh, B. S. Creaven, É. A. Enyedy, *Bioorg. Chem*., **52**, 16–23 (2014).
13. A. Garg, D. M. Manidhar, M. Gokara, C. Malleda, C. S. Reddy, R. Subramanyam, *PLoS One*, **8**, 5, e63805 (2013).
14. D. P. Yeggoni, M. Gokara, D. Mark Manidhar, A. Rachamallu, S. Nakka, C. S. Reddy, R. Subramanyam, *Mol. Pharm.*, **11**, No. 4, 1117–1131 (2014).
15. O. Trott, A. J. Olson, *J. Comput. Chem*., **31**, No. 2, 455–461 (2010).
16. G. M. Morris, D. S. Goodsell, R. S. Halliday, R. Huey, W. E. Hart, R. K. Belew, A. J. Olson, *J. Comput. Chem.*, **19**, No. 14, 1639–1662 (1998).
17. E. Lindahl, B. Hess, D. Van Der Spoel, *Mol. Model. Annual*, **7**, No. 8, 306–317 (2001).
18. A. W. Schüttelkopf, D. M. Van Aalten, *Acta Crystallogr. D: Biol. Crystallogr*., **60**, No. 8, 1355–1363 (2004).
19. W. F. van Gunsteren, X. Daura, A. E. Mark, *Encyclopedia of Computational Chemistry*, **2** (2002).
20. A. Farasat, F. Rahbarizadeh, G. Hosseinzadeh, S. Sajjadi, M. Kamali, A. H. Keihan, *J. Biomol. Struct. Dynam*., **35**, No. 8, 1710–1728 (2017).
21. J. Min, X. Meng-Xia, Z. Dong, L. Yuan, L. Xiao-Yu, C. Xing, *J. Mol. Struct*., **692**, No. 1, 71–80 (2004).
22. G. Zhang, Q. Que, J. Pan, J. Guo, *J. Mol. Struct.*, **881**, No. 1, 132–138 (2008).
23. C. N. Pace, J. M. Scholtz, *Protein Struct.: A Practical Approach*, **2**, 299–321 (1997).
24. R. A. Deshpande, M. I. Khan, V. Shankar, *Biochim. Biophys. Acta - Proteins Proteomics*, **1648**, No. 1, 184–194 (2003).
25. H. Asghari, K. G. Chegini, A. Amini, N. Gheibi, *Int. J. Biol. Macromolecules*, **84**, 35–42 (2016).
26. Z. Chi, R. Liu, Y. Teng, X. Fang, C. Gao, *J. Agric. Food Chem*., **58**, No. 18, 10262–10269 (2010).
27. S. Patel, A. Datta, *J. Phys. Chem. B*, **111**, No. 35, 10557–10562 (2007).
28. G. Zhang, B. Keita, C. T. Craescu, S. Miron, P. de Oliveira, L. Nadjo, *J. Phys. Chem. B*, **111**, No. 38, 11253–11259 (2007).
29. M. Gokara, V. V. Narayana, V. Sadarangani, S. R. Chowdhury, S. Varkala, D. B. Ramachary, R. Subramanyam, *J. Biomol. Struct. Dynam.*, **35**, No. 10, 2280–2292 (2017).
30. R. M. Abreu, H. J. Froufe, M. J. R. Queiroz, I. C. Ferreira, *Chem. Biol. Drug. Des*., **79**, No. 4, 530–534 (2012).
31. V. Mohan, A. C. Gibbs, M. D. Cummings, E. P. Jaeger, R. L. DesJarlais, *Curr. Pharm. Design*, **11**, No. 3, 323–333 (2005).
32. C. Cao, G. Wang, A. Liu, S. Xu, L. Wang, S. Zou, *Int. J. Mol. Sci*., **17**, No. 3, 333 (2016).
33. T. Awang, N. Wiriyatanakorn, P. Saparpakorn, D. Japrung, P. Pongprayoon, *J. Biomol. Struct. Dynam*., **35**, No. 4, 781–790 (2017).
34. G. P. Amini, F. Goshadrou, H. A. Ebrahim, P. Yaghmaei, T. S. Hesami, *Iran. Red. Cresc. Med. J*., **19**, No. 3, e40306 (2017).
35. M. C. Deller, L. Kong, B. Rupp, *Acta Crystallogr. F: Struct. Biol. Commun*., **72**, No. 2, 72–95 (2016).
36. P. Hammarström, B. H. Jonsson, *Protein denaturation and the denatured state. Encyclopedia of Life Sciences*, Wiley, New York (2005).
37. F. Rashid, S. Sharma, B. Bano, *Protein J*., **24**, No. 5, 283–292 (2005).
38. W. K. Lim, J. Rösgen, S. W. Englander, *Proc. Natl. Acad. Sci*., **106**, No. 8, 2595–2600 (2009).
39. R. Capomaccio, I. Osório, I. Ojea-Jiménez, G. Ceccone, P. Colpo, D. Gilliland, R. Hussain, G. Siligardi, F. Rossi, S. Ricard-Blum, *Biointerphases*, **11**, No. 4, 04B310 (2016).
40. H. Xu, N. Yao, H. Xu, T. Wang, G. Li, Z. Li, *Int. J. Mol. Sci*., **14**, No. 7, 14185–14203 (2013).
41. J. W. Donovan, *J. Biol. Chem*., **244**, No. 8, 1961–1967 (1969).
42. B. Ahmad, S. Parveen, R. H. Khan, *Biomacromolecules*, **7**, No. 4, 1350–1356 (2006).
43. H. Zhang, P. Wu, Y. Wang, J. Cao, *Int. J. Biol. Macromol.*, **92**, 593–599 (2016).